AD-A161 960 AN INTERPRETATION OF THE O2 AUGER ELECTRON SPECTRUM(U) 1/1
GEORGE WASHINGTON UNIV WASHINGTON D C DEPT OF CHEMISTRY
H SAMBE ET AL. OCT 85 TR-20 N00014-80-K-0852

UNCLASSIFIED F/G 7/4 NL

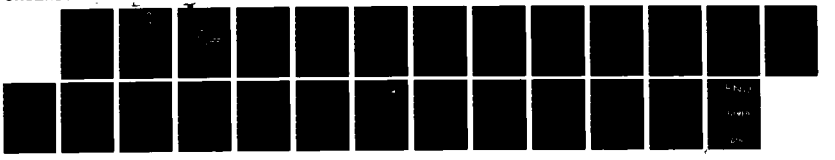

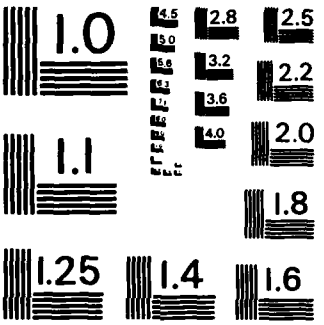

Unclassified

SECURITY CLASSIFICATION OF THIS PAGE (When Data Entered)

REPORT DOCUMENTATION PAGE		READ INSTRUCTIONS BEFORE COMPLETING FORM
1. REPORT NUMBER: No. 20	2. GOVT ACCESSION NO.	3. RECIPIENT'S CATALOG NUMBER
4. TITLE (and Subtitle): AN INTERPRETATION OF THE O_2 AUGER ELECTRON SPECTRUM		5. TYPE OF REPORT & PERIOD COVERED: Technical Report
		6. PERFORMING ORG. REPORT NUMBER
7. AUTHOR(s): Hideo Sambe and David E. Ramaker		8. CONTRACT OR GRANT NUMBER(s): N00014-80-K-0852
9. PERFORMING ORGANIZATION NAME AND ADDRESS: Chemistry Department, George Washington University, Washington, D.C. 20052		10. PROGRAM ELEMENT, PROJECT, TASK AREA & WORK UNIT NUMBERS: Prog. Elem. No. 61153N, Task Area No. PP 013-08-01, Work Unit # NR 056-681
11. CONTROLLING OFFICE NAME AND ADDRESS: Office of Naval Research, Dept. of Navy, 800 N. Quincy Street, Washington, D.C. 22217		12. REPORT DATE: Oct. 1985
		13. NUMBER OF PAGES: 38
14. MONITORING AGENCY NAME & ADDRESS(if different from Controlling Office)		15. SECURITY CLASS. (of this report): Unclassified
		15a. DECLASSIFICATION/DOWNGRADING SCHEDULE

16. DISTRIBUTION STATEMENT (of this Report)

This document has been approved for public release and sale; its distribution is unlimited.

17. DISTRIBUTION STATEMENT (of the abstract entered in Block 20, if different from Report)

18. SUPPLEMENTARY NOTES

Submitted for publication in Chemical Physics.

19. KEY WORDS (Continue on reverse side if necessary and identify by block number)

Oxygen; Auger Spectroscopy; shakeup; photoelectron spectroscopy.

20. ABSTRACT (Continue on reverse side if necessary and identify by block number)

The Auger electron spectrum of O_2 is interpreted by comparing with other spectra, such as the photoelectron spectrum, the electron impact mass spectrum, and the double charge transfer spectrum. Each of these four spectra obeys their own selection rules; the difference in the selection rules plays a key role in our interpretation. Auger decays following a core shake-up excitation are identified for the first time. Many of the previous assignments are revised.

Keywords:

DD FORM 1 JAN 73 1473 EDITION OF 1 NOV 65 IS OBSOLETE S/N 0102-014-6601

Unclassified

SECURITY CLASSIFICATION OF THIS PAGE (When Data Entered)

(12)

OFFICE OF NAVAL RESEARCH

N00014-80-K-0852

Task No. 056-681

Technical Report No. 20

AN INTERPRETATION OF THE O_2 AUGER ELECTRON SPECTRUM

By

Hideo Sambe and David E. Ramaker

Prepared for Publication

in

Chemical Physics

George Washington University
Department of Chemistry
Washington, D.C. 20052

October 1985

DISCLAIMER NOTICE

THIS DOCUMENT IS BEST QUALITY PRACTICABLE. THE COPY FURNISHED TO DTIC CONTAINED A SIGNIFICANT NUMBER OF PAGES WHICH DO NOT REPRODUCE LEGIBLY.

An Interpretation of the O_2 Auger Electron Spectrum *

Hideo Aoyagi and David L. Yeager

Chemistry Department, George Washington University

Washington, DC 20052, USA

* Supported by the Office of Naval Research

Abstract

The Auger electron spectrum of O_2 is interpreted by comparing with other spectra, such as the photoelectron spectrum, the electron impact mass spectrum, and the double charge transfer spectrum. Each of these four spectra obeys their own selection rules; the difference in the selection rules plays a key role in our interpretation. Auger decays following a core shake-up excitation are identified for the first time. Many of the previous assignments are revised.

1. Introduction

First Siegbahn et al. [1] and later Moddeman et al. [2] measured the Auger Electron Spectrum (AES) of O_2 with electron impact. The two spectra agree well in detail. Figure 1 is the O_2 AES measured by Siegbahn et al.. The R1 band, which is drawn with a broken line, is taken from Moddeman's spectrum. In this paper, we assign the Auger transitions, their initial and final states, to the labelled Auger lines of Figure 1.

There are a few calculations on the O_2 AES. Hurley [3] calculated the O_2^{++} state energies by scaling the isoelectronic system N_2. His method yielded accurate energies for the CO^{++}, N_2^{++}, and NO^{++} states [3]. Keebe et al. [4] calculated the O_2^{++} potential curves by the minimal basis ion valence CI method. Dunlap et al. [5] calculated the O_2^{++} state energies, the Auger transition probabilities, and the Auger line widths using the X_α-method. Recently, Gregoritch and Hayes [6] calculated the O_2^{++} state energies and the Auger transition probabilities also using the X_α-method. These X_α calculations cannot distinguish the various multiplet states arising from an electronic configuration.

Previous assignments of the O_2 AES were based on the calculations mentioned above. Siegbahn et al. [1] and Moddeman et al. [2] based their assignments on the O_2^{++} state energies calculated by Hurley [3]. Auger transition probability calculations were not available to them. Dunlap et al. [5] based their assignments on their own calculations, and so did Gregoritch and Hayes [6]. Assignments based on the X_α-calculations have serious problems, since the individual multiplet states are not distinguished. These early assignments disagree with each other more often than they agree.

The present assignments of the O_2 AES are based on the various spectroscopic data. The Fe-W Auger processes, which are defined in the following paragraph, are identified with the PhotoElectron Spectrum (PES). The F-WW Auger processes are identified with the Electron Impact Mass Spectrum (EIMS) and with the Double Charge Transfer Spectrum (DCTS). Differences in the selection rules for the three spectra give clues to the assignments. Finally, the FWe-WW Auger processes are identified by using the core-level PES.

To classify Auger processes in general, we adopt the notations by Moddeman et al. [2]. They are defined as:

Fe-W: Resonant core electron excitation into a one-hole, one-electron (Fe) state, followed by an Auger decay into a one-hole (W) state.

Fe-WWe: Resonant core electron excitation into a one-hole, one-electron (Fe) state, followed by an Auger decay into a two-hole, one-electron (WWe) state.

F-WW: Core electron ionization into a one-hole (F)

state, followed by an Auger decay into a two-hole (WW) state.

(We-WW: Core electron ionization into a two-hole, one-electron (We) state, followed by an Auger decay into a two-hole (WW) state.

The capital letters W and W stand for a core and a valence hole, and the small letter e stands for valence electron.

To classify electronic configurations in general, we adopt the conventional notation, that is, mh-ne for m-hole, n-electron. For instance, we write the 3h-2e configuration for the 3-hole, 2-electron configuration; 2h-1e states for 2-hole, 1-electron states; and the 2h state for the 2-hole state.

2. R1 - R7 Lines

Lines R1, R2, ..., R7 in Fig. 1 behave differently from the rest. These lines are present in the electron-impact (E.E.=5keV) AES as shown in Fig. 1, but they are absent in the photon-impact (hν=1487eV) AES [2]. From this, we can conclude that the R lines originate from a neutral, discrete, core-excited state [2], that is, from Ke-W or Ke-WWe processes.

High-energy (2keV) electron-impact excitation probabilities to the neutral discrete states have been measured by EELS (electron energy loss spectra) [7,8]. These spectra show that the excitation to the $1\sigma_u^{-1}1\pi_g(^3\Pi_u)$

state at 536.8eV above the ground state predominates. We expect therefore that the R lines originate from this $1\sigma_u^{-1}1\pi_g(^3\Pi_u)$ state.

The final states of the $1\sigma_u^{-1}1\pi_g$-AES and the PES are identical; in other words, the final-state binding energies of these two spectra should agree with each other. Figure 2 compares the final-state binding energies obtained from the $1\sigma_u^{-1}1\pi_g$-AES [1], the $^3\Sigma_g^-$-PES [9], and the $^1\Delta_g$-PES [10]. The $1\sigma_u^{-1}1\pi_g$-AES is the R line portion of the AES (Fig. 1). The $^3\Sigma_g^-$-PES is the normal PES; that is, its initial state is the O_2 ground state, $^3\Sigma_g^-$. The initial state of the $^1\Delta_g$-PES is the O_2 first excited state, $^1\Delta_g$. All spectra are plotted against the final-state binding energies, which are measured relative to the O_2 ground state energy.

The R lines of the $1\sigma_u^{-1}1\pi_g$-AES agree (less than 0.2eV difference) with the bands of the two PES as shown in Fig. 2. This is true not only for the peak positions but also for the line shapes. The broad R1 line (≈13eV), which Fig. 2 does not show, also agrees with the first band (12.5eV) of the $^3\Sigma_g^-$ PES [9]. These agreements imply the following:

(a) The initial state of the R lines is indeed the $1\sigma_u^{-1}1\pi_g(^3\Pi_u)$ state.

(b) The final states of the R lines are all one-hole states, whose electronic configurations, symmetries, and usual designations [9] are listed in Table 1.

(c) The measured energies, that is, the $1\sigma_u^{-1}1\pi_g(^3\Pi_u)$ state energy (530.8eV) [1] and the Auger electron kinetic energies measured by Siegbahn et al. [1], are accurate to within ±0.2eV.

Previously the K lines were assigned by Moddeman et al. [2]. They assigned the K1 line to the Fe-W process and the K2-K7 lines to the Fe-WWe process. However we have found that not only the K1 line but also the K2-K7 lines are due to the Fe-W process.

3. N1 - N9 lines

3.1. Various spectra for O_2^{**} states

The O_2^{**} states are reflected in various spectra, such as the Auger Electron Spectrum (AES), the Double Charge Transfer Spectrum (DCTS), and the Electron Impact Mass Spectrum (EIMS). In the following, we shall describe how these three spectra provide O_2^{**} information, emphasizing the selection rules.

3.1.1. Double charge transfer spectrum

When protons of a fixed translational energy collide with O_2 molecules, a single photon can remove two electrons from a molecule and become an H^- ion. A translational energy distribution of the H^- ions gives a double charge transfer spectrum.

From the energy conservation for the process,

$$H^+ + O_2 \rightarrow H^- + O_2^{**} \qquad (1)$$

we have

$$E(O_2^{**}) - E(O_2) = T(H^+) - T(H^-) + E(H^+) - E(H^-) + T(O_2) - T(O_2^{**}) \qquad (2)$$

where T(M) denotes the translational energy of M, and E(M), the internal energy of M.

It is shown [1] that the H^- ions are formed in its ground state; therefore, $E(H^+)-E(H^-)=14.35eV$. The recoil energy of O_2^{**} is negligible; that is, $T(O_2)=T(O_2^{**})$. Substituting these two equations into Eq.(2), we have

$$E(O_2^{**}) - E(O_2) = T(H^+) - T(H^-) + 14.35eV \qquad (3)$$

In this equation, $E(O_2)$ is the O_2 ground state energy, and $T(H^+)$ is a fixed translational energy. Thus, we get the O_2^{**} state energies, $E(O_2^{**})$, by measuring the translational energies of the H^- ions, $T(H^-)$.

Two single-charge transfers,

$$H^+ + O_2 \rightarrow H + O_2^+$$
$$H + O_2 \rightarrow H^- + O_2^+ \qquad (4)$$

also produce the H^- ions. The H^- ion yield by this process, however, depends quadratically on the O_2 gas pressure, while the H^- ion yield by the process (1) depends linearly. From two H^- spectra of different gas pressures, we can learn which peaks are due to the process (1). All DEIS peaks in Fig. 3 are due to the process (1) [12].

The O_2^{**} states formed via the process (1) are triplets, because the proton H^+ is a singlet; the O_2 is in its ground state, $^3\Sigma_g^-$; the H^- ion is formed in its ground state, $^1S_0$; and the total spin of each side of the process (1) must be the same. According to an approximate symmetry selection rule [12], the probability of forming the $O_2^{**}(^3\Sigma_u^+)$ states via the process (1) is small. Furthermore, there is a trend that the lower the energy of O_2^{**}, the higher the probability of its formation.

3.1.1. Electron impact mass spectrum

In electron impact mass spectroscopy, the O_2^{**} ions produced by the process

$$O_2 + e \longrightarrow O_2^{**} + 2e \qquad (5)$$

are counted as a function of the incident electron energy. Near the threshold energy, the square root of the O_2^{**} yield is a linear function of the incident electron energy [13]. Therefore, an extrapolation of $[O_2^{**}]^{1/2}$ to zero yield gives

the threshold energy, or the ground state energy of O_2^{**}. On the other hand, breaks in the O_2^{**} spectrum give excited state energies of O_2^{**}.

The O_2^{**} states formed via the process (5) can be singlet, triplet, quintet, or septuplet; and can have any symmetries.

The EIMS in Fig. 3 was measured by Daly and Powell [14]. They used the charge transfer reaction $O_2^{**}+N_2 \longrightarrow O_2^{+}+N_2^{+}$ to detect the O_2^{**} ions. The EIMS in Fig. 3 shows the $[O_2^{**}]^{1/2}$ plot against the incident electron energy. The zero of the O_2^{**} yield is indicated by a short horizontal line.

3.1.2. Auger electron spectrum

When a core electron, $1\sigma_g$ or $1\sigma_u$, is removed from O_2, the $^2\Delta$, $^2\Sigma^+$, $^4\Sigma^-$, and $^2\Sigma^-$ states are formed. Only the $^4\Sigma^-$ and $^2\Sigma^-$ states, however, can be populated by removing a core electron from the O_2 ground state $^3\Sigma_g^-$, because of the selection rule based on a single configuration. The binding energies of these two states are 543.1eV ($^4\Sigma^-$) and 544.2eV ($^2\Sigma^-$) [1] and are separated by 1.1±0.1eV [1,15]. When excited with high-energy photons (2keV) or high-energy electrons (5keV), these two states have the relative populations, 2.5 ($^4\Sigma^-$) : 1 ($^2\Sigma^-$) [1,15]. These $^4\Sigma^-$ and $^2\Sigma^-$ states are the initial states of the K-WW Auger processes. To get the O_2^{**} state energy from an Auger transition

energy, we have to know from which initial state the Auger transition starts.

Auger transitions from the $^4\Sigma^-$ and $^2\Sigma^-$ states to an identical final state form a pair of Auger lines that satisfy the following three requirements:

(a) The separation of the lines is 1.1±0.1eV.

(b) The widths of the two lines are almost the same.

(c) The line from the $^4\Sigma^-$ state is much stronger than the line from the $^2\Sigma^-$ state.

Three pairs of Auger lines, (N1,N2), (N5,N6), and (N8,N9), satisfy the above three requirements, as shown in Figure 4. These three Auger-line pairs therefore apparently arise from Auger transitions from the $^4\Sigma^-$ and $^2\Sigma^-$ states to an identical final state.

For an allowed Auger transition, the initial state and the final state that includes the outgoing electron must have the same spin and the same symmetry. The selection rules for the final (ionized) state, which does not include the outgoing electron, are the following:

(a) The allowed spins of the final states, that decay from the initial state with spin S, are |S-1/2| and |S+1/2|.

(b) The allowed symmetries of the final states, that decay from the initial state with symmetry Σ^+ (or Σ^-), are any symmetries but Σ^- (or Σ^+).

These selection rules arise because the outgoing electron

orbital, like any other orbital, must have spin 1/2 and any symmetry but Σ^-. From these selection rules, we can draw two conclusions:

(a) The final states of the paired Auger transitions must be triplets, because only the transitions, $^4\Sigma^- \rightarrow$ singlet or triplet and $^4\Sigma^- \rightarrow$ triplet or quintet, are allowed.

(b) The final states of the Auger lines N1-N9 cannot have the Σ^+ symmetry, because a $\Sigma^- \rightarrow \Sigma^+$ transition is forbidden.

3.2. Comparison of AES with EIMS and DCIS

Figure 3 compares the O_2^{++} state energies obtained from EIMS, DCIS, and AES. The O_2^{++} state energies are measured relative to the O_2 ground state energy.

The lowest O_2^{++} (35.3eV) state is observed only in EIMS. In DCIS and AES, transitions to this state are forbidden, because this state has the $^1\Sigma_g^+(1\pi_g^{-2})$ symmetry [3-6].

The second lowest O_2^{++} (40.8eV) state is observed in EIMS as a bread and in DCIS as a shoulder, but not in AES. In AES, transitions to this state are forbidden, because this state has the $^3\Sigma_u^-(1\pi_u^{-1}3\sigma_g^{-1})$ symmetry [3,4]. In DCIS, we might expect, based on the magnitude of transferred energy, that the first band (40.8eV) should be much stronger than the second band (42.6eV). But in reality, the first

[illegible] weaker [illegible] the second band, because the transition to the [illegible] state is approximately forbidden in [illegible] the appropriate symmetry selection rule [1,3].

The third lowest O_2^{**} [illegible] state is observed in [illegible] the strongest peak, [illegible] the strongest paired Auger line [illegible] and possibly in [illegible] is a weak [illegible]. This O_2^{**} state must be a triplet.

The O_2^{**} states at [illegible] eV and [illegible] eV are observed [illegible] shoulders and [illegible] the [illegible] and [illegible] lines. [illegible] initial state of the [illegible] and [illegible] lines must be the [illegible] state in order to agree with the [illegible]. These O_2^{**} states are triplets [illegible].

[illegible] O_2^{**} [illegible] triplet. [illegible] suggested pairing the [illegible] and [illegible] lines instead of pairing the [illegible] and [illegible] lines. However, if we paired the [illegible] and [illegible] lines, we would not have the Auger lines [illegible] in the DLIS. Furthermore, the [illegible] pairing does not satisfy the line width and the line separation requirements given in subsection [illegible].

The O_2^{**} state at [illegible] eV is observed in DLIS as a shoulder and in [illegible] as the [illegible] line. The initial state of the Auger transition causing the N7 line is most likely the

[illegible] state for [illegible]. The [illegible] show the presence of a band between [illegible] and [illegible] indicating that the [illegible] line is a triplet. [illegible] and [illegible] initial state [illegible] triplet state, but the [illegible] state gives a stronger [illegible] than the [illegible] state. If the [illegible] line arose from the [illegible] state, a line stronger than the N7 line would exist between the [illegible] and the [illegible] lines contrary to Figure 4.

The O_2^{**} state at [illegible] eV is observed in DLIS as a shoulder and in [illegible] as the second strongest paired Auger line [illegible], this O_2^{**} state must be a triplet.

[illegible] Electron configurations and symmetries of the [illegible] O_2^{**} states

[illegible] assignment [illegible] listed in Table [illegible] along with the O_2^{**} state energies and the spectroscopic evidence for the O_2^{**} states. The reasons for our assignments [illegible] in the following three subsections.

[illegible].1. The O_2^{**} state energies

In the preceding section, we have shown that the observed O_2^{**} states are triplets except for the lowest state. The order of the assigned triplet states (Table 2) agrees with the order of the lowest six triplet states calculated by Beebe et al. [4].

The triplet states that have been observed in the isoelectronic systems N_2 [16,17] and NO^+ [18] correlate well with the triplet states of O_2^{++}, as shown in Figure 5. The O_2^{++} potential curves are constructed from the calculated internuclear distances [3] and the observed state energies. In the N_2 and NO^+ spectra, the states corresponding to $1\pi_u\ ^2(^3\Delta_g)$ and $2\sigma_u\ ^1 1\pi_u\ ^1(^3\Pi_g)$ have not been observed, because these states can be reached only by a two-electron jump from the ground states of N_2 and NO^+.

Finally the assigned triplet state energies agree very well with those calculated by Hurley [3]. He has not calculated the $O_2^{++}(^3\Delta_u)$, $O_2^{++}(1\pi_u\ ^2)$, and $O_2^{++}(2\sigma_u^{-1}1\pi_u^{-1})$ state energies.

3.3.2. Auger-line widths

An Auger-line width is closely related to the internuclear distance (r_e) of the Auger final state: the smaller the difference between the r_e's of the Auger final state and the ground state, the narrower the Auger line. The $1\pi_u\ ^1 1\pi_g^{-1}$, $3\sigma_g^{-1}1\pi_g^{-1}$, and $2\sigma_u^{-1}1\pi_u^{-1}$ states are expected to have r_e's similar to the ground state, while the $2\sigma_u^{-1}1\pi_g^{-1}$ state is expected to have an r_e considerably smaller than the ground state and the $1\pi_u\ ^2$ state, an r_e much larger than the ground state. (These estimates are based on the $1\pi_u$ and $3\sigma_g$ bonding and $1\pi_g$ and $2\sigma_u$ antibonding characters of the orbitals involved.) Thus, we expect that the N2 ($1\pi_u^{-1}1\pi_g^{-1}$), N3 ($3\sigma_g^{-1}1\pi_g^{-1}$), and N9 ($2\sigma_u^{-1}1\pi_u^{-1}$)

lines should be narrower than the N6 ($1\pi_u\ ^2$) and N7 ($2\sigma_u\ ^1 1\pi_g\ ^1$) lines. This agrees with Figures 1 and 4, supporting our assignments.

Gregoritch and Hayes [6] assigned the $3\sigma_g^{-1}1\pi_u^{-1}$ configuration to the N9 line. The $3\sigma_g\ ^1 1\pi_u\ ^1$ configuration is expected to have an r_e considerably larger than the ground state r_e. This implies that the N9 line should be wider than the N2 line, contrary to Figures 1 and 4. For this reason, we prefer to assign the $2\sigma_u^{-1}1\pi_u^{-1}$ state to the (N8, N9) Auger lines.

Hurley's calculations [3] have shown that the r_e for the $3\sigma_g^{-1}1\pi_g^{-1}$ state is the closest to that for the ground state; the r_e for the $1\pi_u\ ^1 1\pi_g^{-1}$ states, the second closest; and the r_e for the $2\sigma_u^{-1}1\pi_g\ ^1$ state, the third closest; as can be seen in Figure 5. This would predict that the N3 line due to $3\sigma_g\ ^1 1\pi_g^{-1}$ is the narrowest; the N1 and N2 lines due to $1\pi_u^{-1}1\pi_g^{-1}$, the second narrowest; and the N7 line due to $2\sigma_u\ ^1 1\pi_g^{-1}$ state, the third narrowest among these lines. This ordering of the line widths agrees with the line widths observed in Figure 4.

3.3.3. Auger line intensities

Figure 4 shows that the N1+N2+N4 intensity due to $1\pi_u\ ^1 1\pi_g^{-1}$, the N5+N6 intensity due to $1\pi_u^{-2}$, and the N8+N9 intensity due to $2\sigma_u\ ^1 1\pi_u^{-1}$ are much stronger than the N3 intensity due to $3\sigma_g\ ^1 1\pi_g^{-1}$ or the N7 intensity due to $2\sigma_u$

$^1\pi_g{}^{-1}$. (Although the N7 line appears higher than the N6 line, the N7 line is narrower than the N6 line and sits on the broader N6 line as indicated by a shaded area.) This implies that the Auger transitions into the $1\pi_u{}^1 1\pi_g{}^{-1}$, $1\pi_u{}^{-2}$, and $2\sigma_u{}^1 1\pi_u{}^1$ states are the strongest. There have been two calculations on the Auger line intensities [5,6]. Both calculations have predicted the Auger transitions into the $1\pi_u{}^1 1\pi_g{}^1$, $1\pi_u{}^{-2}$, and $2\sigma_u{}^1 1\pi_u{}^1$ states to be the strongest, supporting our assignments.

Table 2 summarizes the assigned electronic configurations and symmetries of the observed O_2^{++} states.

3.4. Previous interpretations on the N1-N9 Auger lines

Krenbahn et al. [1] suggested that the (N6,N7) Auger transitions originate from the $^3\Sigma$ and $^1\Sigma$ initial states and end at the the identical final state c $^3\Pi_u(1\pi_g{}^{-1}2\sigma_u{}^{-1})$. We do not agree with the (N6,N7) pairing for the reasons given in Section 3.2, but do agree with the N7 line assignment.

Moddeman et al. [3] assigned the paired Auger lines (N1,N2) to a $^3\Sigma_u{}^-(1\pi_u{}^1 1\pi_g{}^1)$ and the paired Auger lines (N8,N9) to c $^3\Pi_u(2\sigma_u{}^1 1\pi_g{}^1)$. The Auger transition to a $^3\Sigma_u{}^-(1\pi_u{}^1 1\pi_g{}^1)$ state is forbidden (Subsection 3.1.3). The assignment of the (N8,N9) pair to the c $^3\Pi_u(2\sigma_u{}^1 1\pi_g{}^{-1})$ state would yield a higher energy for the c $^3\Pi_u$ state (Subsection 3.1.1), larger Auger-line widths for the narrow

N8 and N9 lines (Subsection 3.3.2), and smaller Auger line intensities for the strong N8 and N9 lines (Subsection 3.3.3), all inconsistent with observations.

Dunlap et al. [5] assigned the paired Auger lines (N1,N2) to $1\pi_g{}^1 1\pi_u{}^{-1}$,; (N3,N4) to $1\pi_g{}^1 3\sigma_g{}^1$; (N6,N7) to $1\pi_u{}^{-2}$; (N8,N9) to $1\pi_u{}^1 2\sigma_u{}^{-1}$; and a single Auger line N5 to $1\pi_g{}^1 2\sigma_u{}^1$. Recall that their calculations cannot distinguish the individual multiplet states. We agree with the (N1,N2) and the (N8,N9) assignments, but disagree with the (N3,N4) and the (N6,N7) pairings for the reasons stated before. We believe, contrary to their assignment, that the N5 line should be paired with the N6 line and assigned to the $1\pi_u{}^{-2}$.

Gregoritch and Hayes [6] assigned the N2 line to $1\pi_g{}^1 1\pi_u{}^{-1}$ and the N9 line to $3\sigma_g{}^{-1} 1\pi_u{}^{-1}$. Like the Dunlap's calculations, their X_α calculations cannot distinguish the individual multiplet states. We agree with the first assignment, but disagree with the second assignment for the reasons given in Subsection 3.3.2.

A summary of our assignments for the N1-N9 Auger lines are listed in Table 1.

4. S1 and S2 lines

The S1 and S2 lines, unlike the R1-R7 lines, appear in the photon-excited (hν=1487eV) AES [2]. This implies that

the S1 and S2 lines do not arise from the W or the WW Auger process, but arise from the WW or the WW Auger process.

4.1. Previous assignments of the S1 and S2 lines

Moddeman et al. [3], Siegbahn et al. [1], and Gregoritch and Hayes [6] have assigned the S1 and S2 lines to the Auger transitions from the $^2\Sigma$ ($1\sigma^1$) and $^4\Sigma$ ($1\sigma^1$) states to the $^1\Sigma_g^+(1\pi_g^2)$ state. This assignment is not acceptable for the following reasons:

(a) The separation (1.6eV) of the S1 and S2 lines does not agree with the separation (1.1eV) of the initial states.

(b) The relative intensity (S2/S1 = 1) of the S1 and S2 lines is not like that of the other paired Auger lines ($N_{4,5}N1 : N_{6,7}N_{4,5}N_{6,7}$ = 1:).

(c) The $U_3^{++}(1\pi_g^2)^1\Sigma_g^+$ state energy (~8.1eV or ~8.4eV as determined by their S1 or S2 assignment respectively) does not agree with that (~5.6eV~ ~7.2eV) measured by electron impact mass spectrometry [14,19,20,21]. We believe that the vertical $U_2^{++}(1\pi_g^2)^1\Sigma_g^+$ state energy is ~6.2±0.5eV.

(d) The Auger transition from the $^2\Sigma^+$ initial state to the $^2\Sigma^+$ final state is forbidden (see Subsection 3.1.3).

Realizing that Auger transitions from quartet to singlet states are forbidden, Dunlap et al. [5] reassigned

the S2 line to the Auger transition from the $U_3^{++}(1\sigma^1)^4\Sigma^-$ state to the $U_3^{++}(1\pi_g^2)^1\Sigma_g^+$ state and the S1 line to a (e-W or a (e-WW) Auger process. This assignment is also not acceptable for the following reasons:

(a) The resulting $U_2^{++}(1\pi_g^2)^1\Sigma_g^+$ state energy (~9.9eV) is far too large in comparison with the e[illegible] state energy (~6.2eV).

(b) The Auger transition from $^2\Sigma^-$ to $^1\Sigma^+$ is forbidden as well as the Auger transition from $^4\Sigma^-$ to $^1\Sigma^+$ (see Subsection 3.1.3).

(c) The S1 line does not arise from a (e-W (or a (e-WW) Auger process, because it appears in the photon-excited (hν=1486.6eV) XPES.

4.2. Our assignment of the S1 and S2 lines

We suspect that the S1 and S2 lines are not due to a (WW process but due to a (We WW process. The core level XPS (1s) of U_3 shows pronounced satellite (shake-up) peaks at [illegible] and 10.7eV above the main $^2\Sigma$ ($1\sigma^1$) peak. We attribute the S1 and S2 lines to the Auger transitions from these two shake-up states to the $U_2^{++}(1\pi_u^2)^1\Delta_g$ state. The reasons for this S1,S2 assignment are as follows:

(a) The separation (1.8eV) of the shake-up peaks agrees with the separation (1.8eV) of the S1 and S2 lines.

(b) The relative intensity (~1) of the shake-up peaks agrees with the relative intensity (~1) of the

S1 and S2 lines.

(c) The relative magnitude between the S1 S2 and the N1-N9 lines is comparable to the relative magnitude between the shake-up and the main peaks.

(d) Among the Auger decays starting from the shake-up state ($1\sigma_u^{-1}1\pi_u^{-1}1\pi_g$), the decay into the $O_2^{++}(1\pi_u^{-2})$ state is expected to be the strongest. (This will be shown in the following paragraph.)

(e) The $O_2^{++}(1\pi_u^{-2})\,^3\Delta_g$ state energy (47.3eV) calculated from the (N5,N6) lines agrees with that (47.7eV) calculated from the (S1,S2) lines. The small difference (0.4eV) between the two calculations is due to the different intermediate states, the main ($1\sigma_u^{-1}$) in the former and the shake-up ($1\sigma_u^{-1}1\pi_u^{-1}1\pi_g$) state in the latter.

(f) A Five-WW Auger transition has been observed in the AES of CO [23].

The 2h final states that can be reached from the initial state $1\sigma_u^{-1}1\pi_u^{-1}1\pi_g$ by an allowed Auger transition are $1\pi_u^{-1}V^{-1}$, where V can be any of $1\pi_g$, $1\pi_u$, $3\sigma_g$, $2\sigma_u$, or $2\sigma_g$. The corresponding Auger transitions are:

$$(1\pi_g,V) \rightarrow (1\sigma,\varepsilon) \quad \text{for } V = 1\pi_g,\ 1\pi_u,\ 3\sigma_g,\ 2\sigma_u,\ 2\sigma_g, \qquad (6)$$

where ε stands for the outgoing electron. The σ^{-1}-AES shows that, among the Auger transitions (6), the transition with $V=1\pi_u$ is by far the strongest. (See Table 2 and Fig. 4, and

recall that the other strong Auger transitions are $(1\pi_u,1\pi_u)$ and $(1\pi_u,2\sigma_u)$.) Therefore, among the Auger decays starting from the shake-up ($1\sigma^{-1}1\pi_u^{-1}1\pi_g$) state, the decay into the $1\pi_u^{-2}$ state is expected to be the strongest. In fact, according to our interpretation, we have observed this decay but not other decays.

Our assignments of the S1 and S2 Auger lines are included in Table 1. Note that the order of the $^4\Sigma^-$ and $^2\Sigma^-$ states arising from $1\sigma^{-1}1\pi_u^{-1}1\pi_g$ is reversed from that of the $^4\Sigma^-$ and $^2\Sigma^-$ states arising from $1\sigma^{-1}$. The reason is given in the Appendix.

5. NS1 - NS3 lines

The broadness of the NS1-NS3 lines is due to CI mixing of the 2h states with 3h-1e states. A large number of 3h-1e states are expected in this energy region. The majority of them are Rydberg states converging to 2h states and are densely distributed. Auger transitions from the $O^*(1\sigma^{-1})$ states into these 3h-1e states are forbidden, since they are three-electron-jump transitions. The intensities of the NS1-NS3 lines are due to 2h states, and the peaks of the NS1-NS3 lines tend to match with the 2h state energies prior to the CI mixing. In this section, we assign the pre-CI 2h states to the NS1-NS3 lines.

Figure 6 compares the O_2-AES [1] with the two NO-AES [2], the nitrogen core ($1s_N^{-1}$) and the oxygen core ($1s_O^{-1}$)

spectra. A sum of the two NO-AES almost reproduces the O_2-AES, as can be seen in Figure 6. The three NS1-NS3 peaks are clearly reproduced by this addition. Our assignment for the NS1-NS3 lines are based on this correspondence between the NO-AES and the O_2-AES.

For the NO-AES assignments, we can use the intensity changes between the $1s_O^{-1}$ and $1s_N^{-1}$ spectra. Furthermore, there is an accurate calculation [24] by the CI method for NO-AES. Our assignments of the NO-AES, details of which will be published elsewhere, are shown in the bottom of Figure 6.

Based on the close correspondence between the NO-AES and the O_2-AES, we assign $2\sigma_u^{-2}$ and $2\sigma_g^{-1}1\pi_g^{-1}$ to the NS1 line, $2\sigma_g^{-1}3\sigma_g^{-1}$ to NS2, and $2\sigma_g^{-1}2\sigma_u^{-1}$ to NS3. Since the assignments are tentative, they are not included in Table 1.

Previously Dunlap et al. [5] assigned $2\sigma_u^{-1}3\sigma_g^{-1}$ to NS1, $2\sigma_g^{-1}1\pi_u^{-1}$ to NS2, and $2\sigma_g^{-1}2\sigma_u^{-1}$ to NS3. Also recently Gregoritch and Hayes assigned $2\sigma_u^{-2}$ to NS1, $2\sigma_g^{-1}1\pi_u^{-1}$ to NS2, and $2\sigma_g^{-1}2\sigma_u^{-1}$ to NS3. The three studies agree on the NS3 assignment, but disagree on the NS1 and NS2 assignments. We believe that the energy of $2\sigma_u^{-1}3\sigma_g^{-1}$ is too low for the NS1 assignment. Also, the $2\sigma_g^{-1}1\pi_u^{-1}$ states may not be observed as a resolved peak, because eight allowed states arise from the $2\sigma_g^{-1}1\pi_u^{-1}$ configuration.

6. Summary

Our assignments of the O_2 Auger electron spectrum are summarized in Table 1. These assignments are confirmed by selection rules, calculations, and other experiments. The assignments of the NS1-NS3 lines are tentative; they are not included in Table 1.

Appendix: Shake-up states of $O_2^+(1\sigma_u^{-1})$

Since shake-up states have 2h-1e configurations, photoionization into shake-up states are forbidden. Shake-up states borrow their photoionization intensity from the 1h states, $^2\Sigma_u^-(1\sigma_u^{-1})$ and $^4\Sigma_u^-(1\sigma_u^{-1})$, through CI mixing. The observed shake-up states in PES, therefore, must have either the $^2\Sigma_u^-$ or $^4\Sigma_u^-$ symmetry.

The lower-lying shake-up states are expected to arise from the electronic configurations, $1\sigma_u^{-1}{}_u{}^1\pi_g$, $1\sigma_u^{-1}3\sigma_g^{-1}{}^1\pi_g$, or $1\sigma_u^{-1}2\sigma_u^{-1}1\pi_g$. The first configuration gives both the $^2\Sigma_u^-$ and $^4\Sigma_u^-$ symmetries, but the second and the third configurations do not give either symmetry. The lowest observed shake-up state, therefore, must arise from the $1\sigma_u^{-1}{}^1\pi_u^{-1}1\pi_g$ configuration.

The $1\sigma_u^{-1}1\pi_u^{-1}1\pi_g$ configuration gives two $^2\Sigma_u^-$ states and one $^4\Sigma_u^-$ state. In Fig. 7, the relative positions of these three states are estimated from the observed $O_2(1\pi_u^{-1}1\pi_g)$ states, c $^1\Sigma_u^-$ and B $^3\Sigma_u^-$ [25,26]. Coupling with the core-hole $1\sigma_u^{-1}$, the $^3\Sigma_u^-$ states (B $^3\Sigma_u^-$ and the ground state $^3\Sigma_g^-$)

split into the $^4\Sigma^-$ and the $^2\Sigma^-$ states. Assuming that the two splittings are the same and that the weighted average of the $^4\Sigma^-$ (4) and $^2\Sigma^-$ (2) state energies gives the $^3\Sigma^-$ state energy, we have obtained the relative positions of the $^2\Sigma^-$ and $^4\Sigma^-$ states. The results are shown in Figure 7.

Two states tend to mix more in CI, when they are closer in energy. Based on this trend, we expect that the lower $^2\Sigma^-$ state is stronger in intensity than the higher $^2\Sigma^-$ state. The $^4\Sigma^-$ state mixes less than the lower $^2\Sigma^-$ state, but the $^4\Sigma^-$ state has the higher multiplicity than the lower $^2\Sigma^-$ state. Considering these factors, we expect that the lower $^2\Sigma^-$ state and the $^4\Sigma^-$ state have about the same intensities in PES and that the higher $^2\Sigma^-$ state is much weaker than the other two.

To sum up, two shake-up peaks due to the lower $^2\Sigma^-(1\sigma^{-1}1\pi_u^{-1}1\pi_g)$ and the $^4\Sigma^-(1\sigma^{-1}1\pi_u{}^{-1}1\pi_g)$ states are expected around 6.9eV and 8.6eV above the main $^4\Sigma^-(1\sigma^{-1})$ peak. These peaks are expected to have similar intensities and to be well separated from the next lowest shake-up peak.

Shake-up peaks are observed at 8.9eV and 10.7eV above the main $^4\Sigma^-(\sigma^{-1})$ peak [1,22]. These peaks have similar intensities and are well separated from the next lowest shake-up peak, which appears around 22eV above the main peak [1,22].

Our estimates and the experiments agree well, especially on the separation of the two peaks: 1.7eV (estimated) and 1.8eV (observed). Based on this agreement, we assign the lower $^2\Sigma^-(1\sigma^{-1}1\pi_u^{-1}1\pi_g)$ state to the 8.9eV peak and the $^4\Sigma^-(1\sigma^{-1}1\pi_u^{-1}1\pi_g)$ state to the 10.7eV peak.

References

[1] K. Siegbahn, C. Nordling, G. Johansson, J. Hedman, P. F. Heden, K. Hamrin, U. Gelius, T. Bergmark, L. O. Werme, R. Manne, and Y. Baer, "ESCA: Applied to Free Molecules" (North-Holland, Amsterdam, 1969).

[2] W. E. Moddeman, T. A. Carlson, M. O. Krause, B. P. Pullen, W. E. Bull, and G. K. Schweitzer, J. Chem. Phys. 55(1971)2317.

[3] A. C. Hurley, J. Mol. Spectrosc. 9(1962)18.

[4] N. H. F. Beebe, E. W. Thulstrup, and A. Anderson, J. Chem. Phys. 64(1976)2080.

[5] B. I. Dunlap, P. A. Mills, and D. E. Ramaker, J. Chem. Phys. 75(1981)300.

[6] S. J. Gregoritch and R. G. Hayes, to be published.

[7] G. R. Wight and C. E. Brion, J. Electron Spectrosc. Relat. Phenom., 4(1974)313.

[8] A. P. Hitchcock and C. E. Brion, J. Electron Spectrosc. Relat. Phenom., 18(1980)1.

[9] O. Edqvist, E. Lindholm, L. E. Selin and L. Asbrink, Physica Scripta. 1(1970)25.

[10] N. Jonathan, A. Morris, M. Okuda, K. J. Ross, and D. J. Smith, Chem. Soc. Farady Transaction II 70(1974) 1810.

[11] J. Durup, J. Appell, F. C. Fehsenfeld, and P. Fournier, J. Phys. B 5(1972)L110; 5(1972)1810.

[12] J. Appell, J. Durup, F. C. Fehsenfeld, and P. Fournier, J. Phys. B 6(1973)197.

[13] G. H. Wannier, Phys. Rev. 100(1955)1180.

[14] N. R. Daly and R. E. Powell, Proc. Phys. Soc. 90(1967)629.

[15] P. S. Bagus, M. Schrenk, D. W. Davis, and D. A. Shirley, Phys. Rev. A 9(1974)1090.

[16] A. Lotthus and M. H. Krupenie, J. Phys. Chem. Ref. Data 6(1977)113.

[17] F. A. Baum and W. M. Benesch, Appl. Opt. 9(1970)195.

[18] O. Edqvist, E. Lindholm, L. E. Selin, H. Sjogren, and L. Asbrink, Arkiv Fysik 40(1969)439.

[19] F. H. Dorman and J. D. Morrison, J. Chem. Phys. 39(1963)1906.

[20] T. D. Mark, J. Chem. Phys. 63(1975)3731.

[21] J. H. Agee, J. B. Wilcox, L. E. Abbey, and T. F. Moran, Chem. Phys. 61(1981)171.

[22] T. A. Carlson, M. O. Krause, and W. E. Moddeman, J. de Physique Colloque C4(1971)76.

[23] L. Ungier and T. D. Thomas, Phys. Rev. Letters 53(1984)435.

[24] H. Agren, J. Chem. Phys. 75(1981)1267.

[25] J. Geiger and B. Schroder, J. Chem. Phys. 49(1968)740.

[26] K. P. Huber and G. Herzberg, "Molecular Spectra and Molecular Structure, IV Constants of Diatomic Molecules" (Van Nostrand Reinhold Co., New York, 1979).

Table 1
Assignment of O_2 Auger electron spectrum

Band	K.E. (eV)	Initial state Config.	Desig.	Final state Config.		Desig.	B.E. (eV)
R1	518.	$1\sigma_u^{-1}1\pi_g$	$^3\Pi_u$	$1\pi_g^{-1}$	X	$^2\Pi_g$	13.
R2	514.1	"	"	$1\pi_u^{-1}$	a	$^4\Pi_u$	16.7
R3	513.1	"	"	"	A	$^2\Pi_u$	17.7
R4	512.2(4)	"	"	$3\sigma_g^{-1}$	b	$^4\Sigma_g^-$	18.6
R5	511.7	"	"	$1\pi_u^{-1}$		$^2\Phi_u$	19.1
R6	510.9(4)	"	"	$3\sigma_g^{-1}$		$^2\Delta_g$	19.9
R7	510.4(4)	"	"	"	B	$^2\Sigma_g^-$	20.4
S1	506.1(5)	$1\sigma^{-1}1\pi_u^{-1}1\pi_g$	$^4\Sigma^-$	$1\pi_u^{-2}$		$^3\Delta_g$	47.7
S2	504.3(4)	"	$^2\Sigma^-$	"		"	"
N1	501.6(3)	$1\sigma^{-1}$	$^2\Sigma^-$	$1\pi_u^{-1}1\pi_g^{-1}$	w	$^3\Delta_u$	42.6
N2	500.5(3)	"	$^4\Sigma^-$	"	"	"	"
N3	499.7(3)	"	"	$3\sigma_g^{-1}1\pi_g^{-1}$	b	$^3\Pi_g$	43.4
N4	499.3(4)	"	"	$1\pi_u^{-1}1\pi_g^{-1}$	b'	$^3\Sigma_u^-$	43.8
N5	496.9	"	$^2\Sigma^-$	$1\pi_u^{-2}$		$^3\Delta_g$	47.3
N6	495.8(4)	"	$^4\Sigma^-$	"		"	"
N7	494.6(4)	"	"	$2\sigma_u^{-1}1\pi_g^{-1}$	c	$^3\Pi_u$	48.5
N8	492.9(4)	"	$^2\Sigma^-$	$2\sigma_u^{-1}1\pi_u^{-1}$		$^3\Pi_g$	51.2
N9	491.9(4)	"	$^4\Sigma^-$	"		"	"

Table 2
Observed O_2^{++} states

Binding Energy (eV)	Electronic Configuration	Designation & Symmetry		Spectroscopy AES	DCIS	EIMS
36.3(5)	$1\pi_g^{-2}$	X	$^1\Sigma_g^+$	f[a]	f	threshold
40.8(2)	$1\pi_u^{-1}1\pi_g^{-1}$	a	$^3\Sigma_u^+$	f	shoulder	break
42.6	$1\pi_u^{-1}1\pi_g^{-1}$	w	$^3\Delta_u$	N1,N2	peak	break(?)
43.4	$3\sigma_g^{-1}1\pi_g^{-1}$	b	$^3\Pi_g$	N3	shoulder	----
43.8	$1\pi_u^{-1}1\pi_g^{-1}$	b'	$^3\Sigma_u^-$	N4	shoulder	----
47.3	$1\pi_u^{-2}$		$^3\Delta_g$	N5,N6	peak	----
48.5	$2\sigma_u^{-1}1\pi_g^{-1}$	c	$^3\Pi_u$	N7	shoulder	----
51.2	$2\sigma_u^{-1}1\pi_u^{-1}$		$^3\Pi_g$	N8,N9	shoulder	----

[a] forbidden transition

Figure Captions

Fig. 1. Electron-impact Auger electron spectrum for O_2 obtained by Siegbahn et al. [1]. The K1 band is taken from Ref. [2]. The labelled lines are assigned in Table 1.

Fig. 2. Comparison of the $1\sigma_u^{-1}1\pi_g$-AES [1] with the $^3\Sigma_g^-$-PES [9] and the $^1\Delta_g$-PES [10]. All three spectra are plotted against the O_2^+ final-state energies, which are measured relative to the O_2 ground state energy.

Fig. 3. Comparison of the $1\sigma^{-1}$-AES [1] with the Electron Impact Mass Spectrum [14] and the Double Charge Transfer Spectrum [12]. All three spectra are plotted against the O_2^{++} state energies, which are measured relative to the O_2 ground state energy. The EIMS shows the square-root plot of the O_2^{++} ion yield. The O_2^{++} state energies of AES are based on the initial state assignments given in Table 1.

Fig. 4. Paired Auger transitions from the $^4\Sigma^-$ and $^2\Sigma^-$ initial states to an identical final state. The paired Auger transitions are connected at the bottom. The shaded area indicates the N5+N6 portion of the spectrum. This spectrum is an expansion of Figure 1.

Fig. 5. Comparison among the isoelectronic states of N_2, NO^+, and O_2^{++}. The broken-line potential curve is the b $^3\Pi_g$ state. The state names used in the NO^+ system [18] are adopted here. The potential curves of N_2 [16,17] and NO^+ [18] are from experiments. The O_2^{++} potential curves are constructed from the calculated internuclear distances [3] and the observed state energies. The vertical broken line for O_2^{++} shows the internuclear distance of the O_2 ground state. The vertical broken lines for the N_2 and NO^+ systems are drawn at the same relative positions as the O_2^{++} system for comparison.

Fig. 6. Comparison of the O_2-AES [1] with the two NO-AES [2], the nitrogen core ($1s_N^{-1}$) and the oxygen core ($1s_O^{-1}$) spectra. Our assignments of the NO-AES are given in the bottom.

Fig. 7. Estimation of the $^2\Sigma^-(1\sigma^{-1}1\pi_u^{-1}1\pi_g^{-1})$ and $^4\Sigma^-(1\sigma^{-1}1\pi_u^{-2}1\pi_g^{-1})$ state energies from the observed c $^1\Sigma_u^-(1\pi_u^{-1}1\pi_g^{-1})$ and B $^3\Sigma_u^-(1\pi_u^{-1}1\pi_g^{-1})$ state energies. The following experimental data are used in the diagram: the vertical excitation energy (8.6eV) of the B $^3\Sigma_u^-$ state [25]; the energy difference (2.1eV) of the c $^1\Sigma_u^-$ and the B $^3\Sigma_u^-$ states [26]; the energy difference (1.1eV) of the main $^4\Sigma^-(\sigma^{-1})$ and $^2\Sigma^-(\sigma^{-1})$ peaks [1,15].

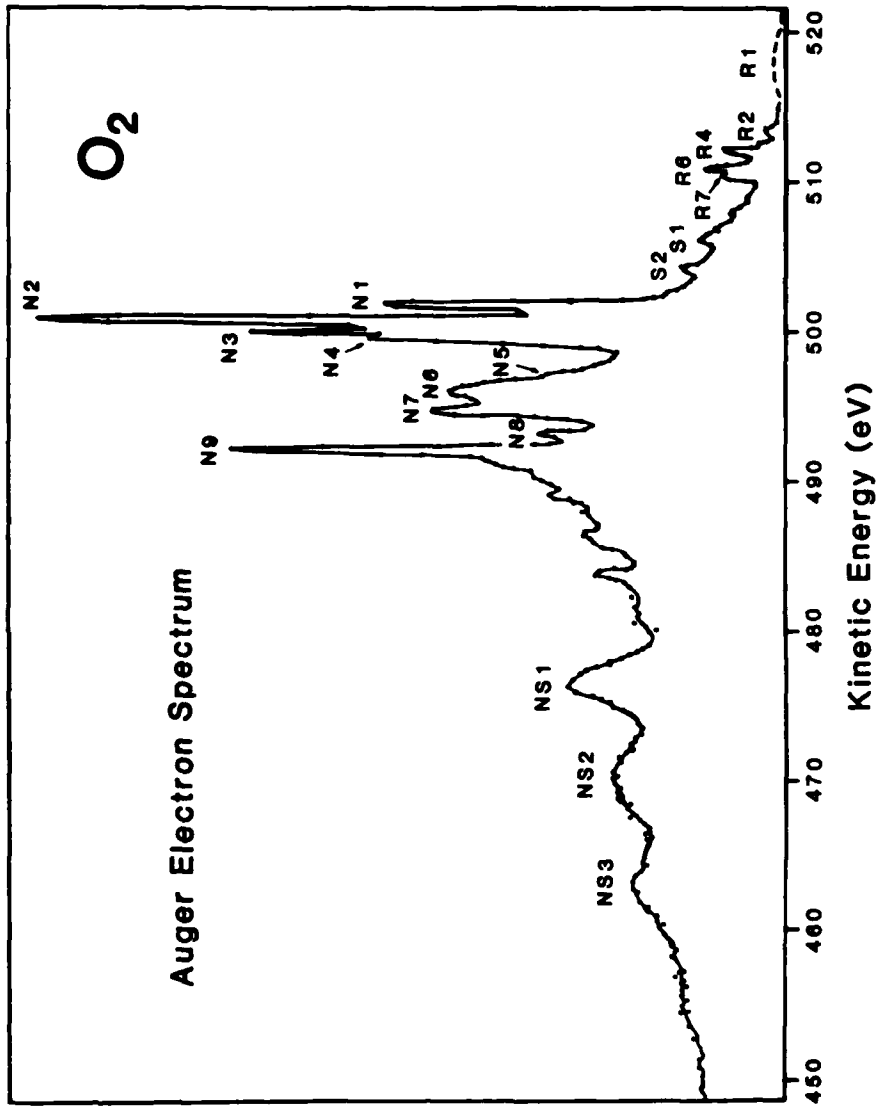
O2
Auger Electron Spectrum
Kinetic Energy (eV)
520
510
500
490
480
470
460
450
N2
N1
N3
N4
N5
N6
N7
N8
N9
NS1
NS2
NS3
S2
S1
R7
R6
R4
R2
R1

Fig. 1

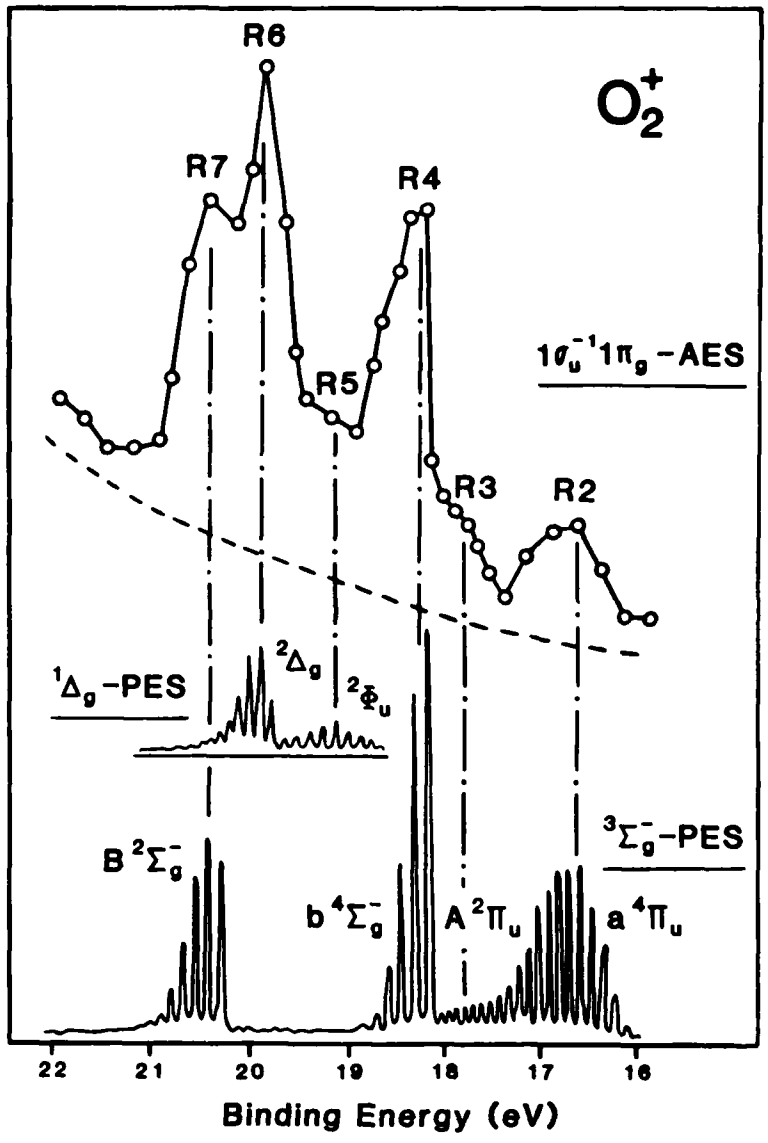
O2+
R6
R7
R4
R5
R3
R2
1σu-1 1πg -AES
1Δg -PES
2Δg
2Φu
B 2Σg-
b 4Σg-
A 2πu
3Σg--PES
a 4πu
22
21
20
19
18
17
16
Binding Energy (eV)

Fig. 2

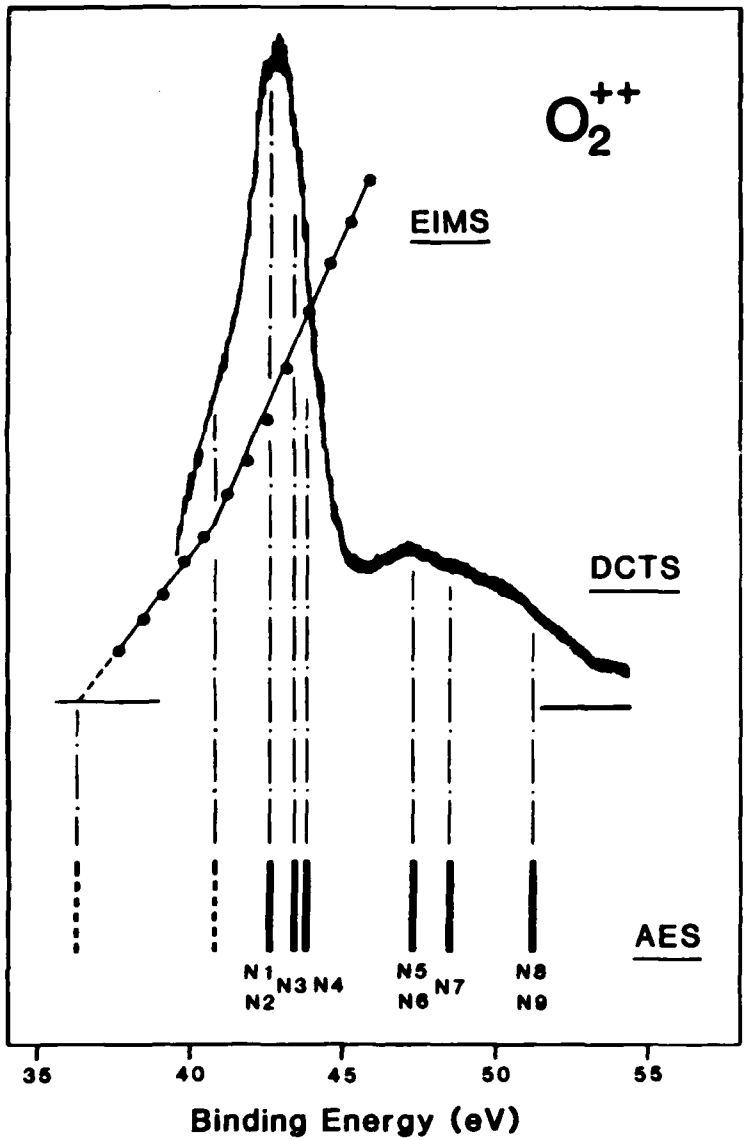
O_2^{++}
EIMS
DCTS
AES
N1
N2
N3
N4
N5
N6
N7
N8
N9
35
40
45
50
55
Binding Energy (eV)

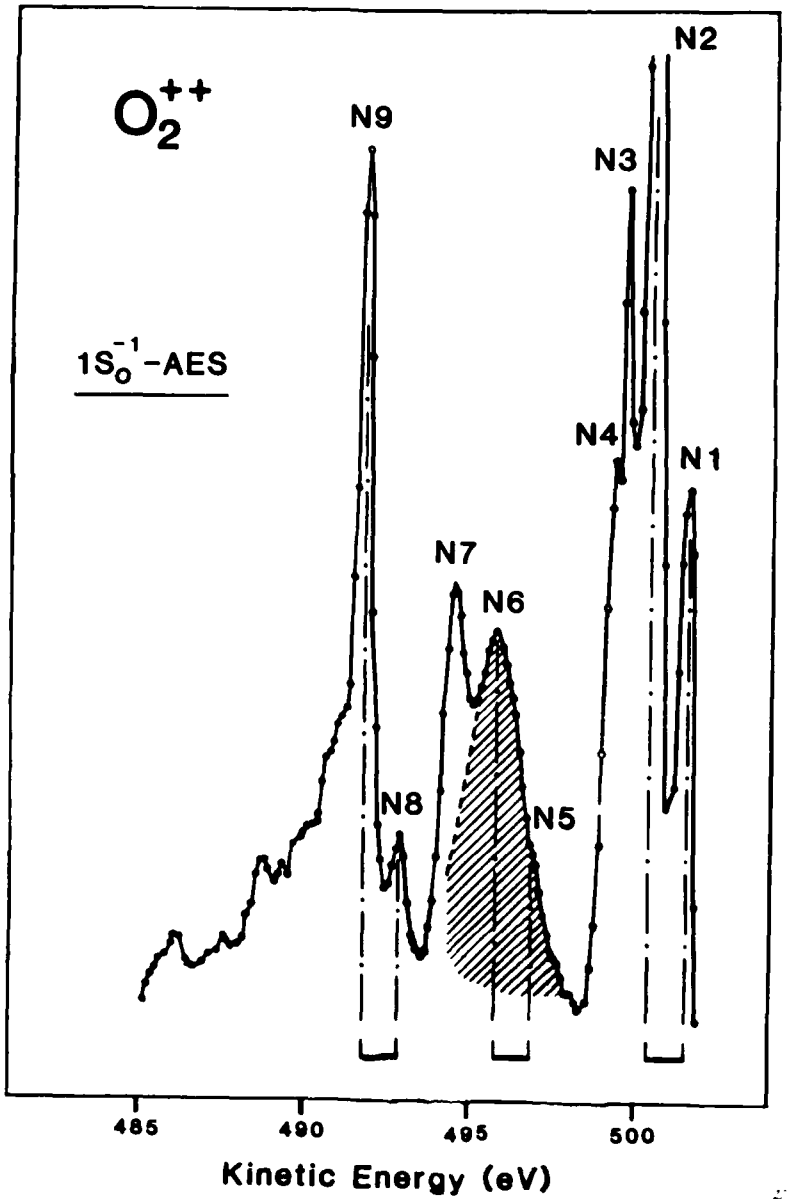
O_2^{++}
$1S_o^{-1}$-AES
N9
N2
N3
N4
N1
N7
N6
N8
N5
485
490
495
500
Kinetic Energy (eV)

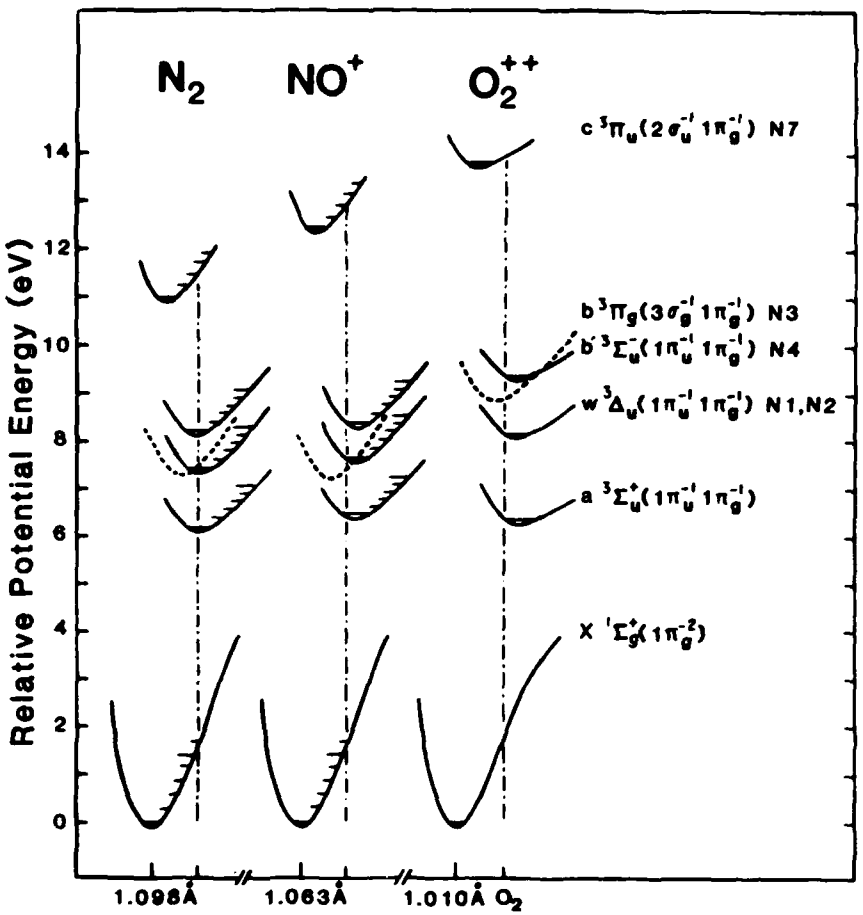
N2
NO+
O2++
Relative Potential Energy (eV)
0
2
4
6
8
10
12
14
c 3πu(2σu-1 1πg-1) N7
b 3πg(3σg-1 1πg-1) N3
b' 3Σu-(1πu-1 1πg-1) N4
w 3Δu(1πu-1 1πg-1) N1,N2
a 3Σu+(1πu-1 1πg-1)
X 1Σg+(1πg-2)
1.098Å
1.063Å
1.010Å O2

Fig. 5

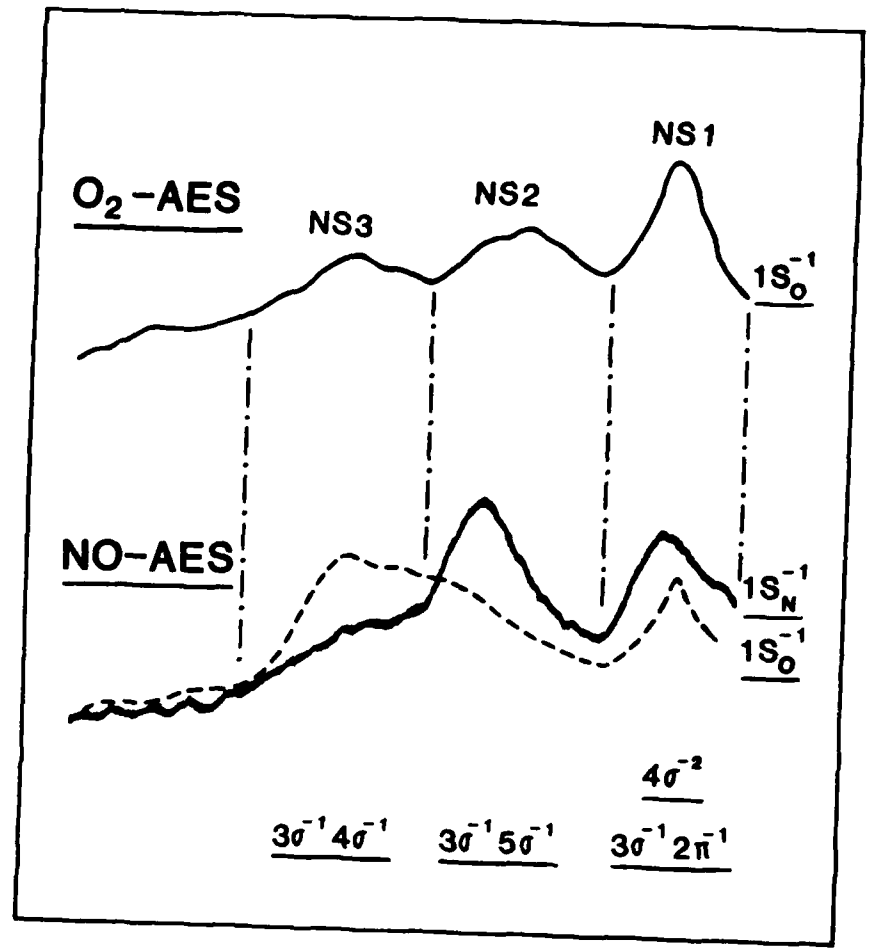
O2-AES
NS3
NS2
NS1
1S0-1
NO-AES
1SN-1
1SO-1
4σ-2
3σ-14σ-1
3σ-15σ-1
3σ-12π-1

Fig. 6

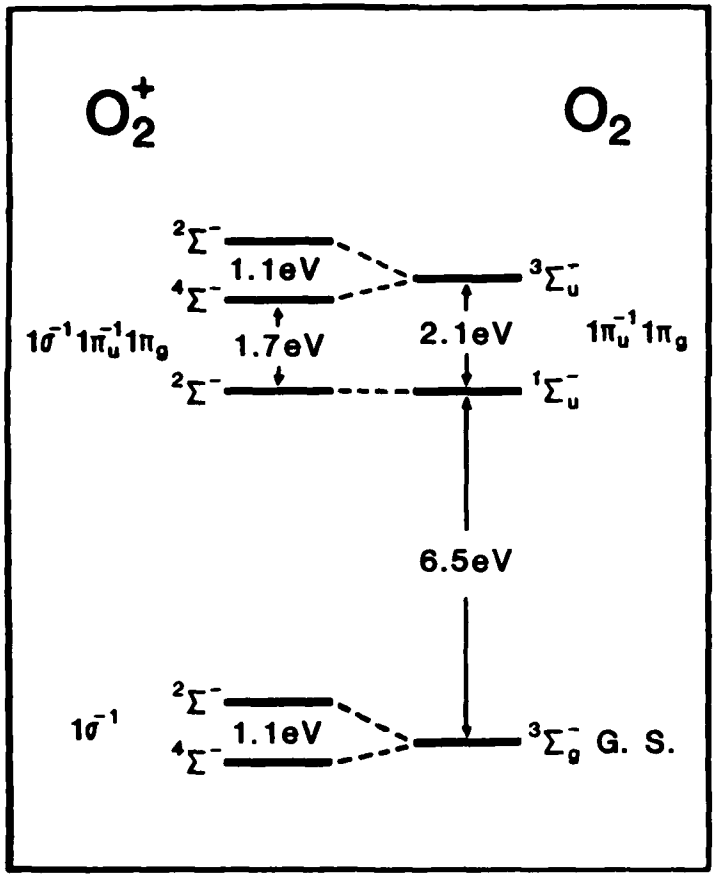
O_2^+
O_2
$^2\Sigma^-$
$^4\Sigma^-$
1.1eV
$^3\Sigma_u^-$
$1\sigma^{-1}1\pi_u^{-1}1\pi_g$
1.7eV
2.1eV
$1\pi_u^{-1}1\pi_g$
$^2\Sigma^-$
$^1\Sigma_u^-$
6.5eV
$1\sigma^{-1}$
$^2\Sigma^-$
$^4\Sigma^-$
1.1eV
$^3\Sigma_g^-$ G. S.

TECHNICAL REPORT DISTRIBUTION LIST, GEN

	No. Copies
Office of Naval Research Attn: Code 413 800 N. Quincy Street Arlington, Virginia 22217	2
Dr. Bernard Douda Naval Weapons Support Center Code 5042 Crane, Indiana 47522	1
Commander, Naval Air Systems Command Attn: Code 310C (H. Rosenwasser) Washington, D.C. 20360	1
Naval Civil Engineering Laboratory Attn: Dr. R. W. Drisko Port Hueneme, California 93401	1
Defense Technical Information Center Building 5, Cameron Station Alexandria, Virginia 22314	12
DTNSRDC Attn: Dr. G. Bosmajian Applied Chemistry Division Annapolis, Maryland 21401	1
Dr. William Tolles Superintendent Chemistry Division, Code 6100 Naval Research Laboratory Washington, D.C. 20375	1
Dr. David Young Code 334 NORDA NSTL, Mississippi 39529	1
Naval Weapons Center Attn: Dr. A. B. Amster Chemistry Division China Lake, California 93555	1
Scientific Advisor Commandant of the Marine Corps Code RD-1 Washington, D.C. 20380	1
U.S. Army Research Office Attn: CRD-AA-IP P.O. Box 12211 Research Triangle Park, NC 27709	1
Mr. John Boyle Materials Branch Naval Ship Engineering Center Philadelphia, Pennsylvania 19112	1
Naval Ocean Systems Center Attn: Dr. S. Yamamoto Marine Sciences Division San Diego, California 91232	1

ABSTRACTS DISTRIBUTION LIST, 056/625/629

Dr. F. Carter
Code 6132
Naval Research Laboratory
Washington, D.C. 20375

Dr. Richard Colton
Code 6112
Naval Research Laboratory
Washington, D.C. 20375

Dr. Dan Pierce
National Bureau of Standards
Optical Physics Division
Washington, D.C. 20234

Dr. R. Stanley Williams
Department of Chemistry
University of California
Los Angeles, California 90024

Dr. R. P. Messmer
Materials Characterization Lab.
General Electric Company
Schenectady, New York 22217

Dr. Robert Gomer
Department of Chemistry
James Franck Institute
5640 Ellis Avenue
Chicago, Illinois 60637

Dr. Ronald Lee
R301
Naval Surface Weapons Center
White Oak
Silver Spring, Maryland 20910

Dr. Paul Schoen
Code 5570
Naval Research Laboratory
Washington, D.C. 20375

Dr. John T. Yates
Department of Chemistry
University of Pittsburgh
Pittsburgh, Pennsylvania 15260

Dr. Richard Greene
Code 5230
Naval Research Laboratory
Washington, D.C. 20375

Dr. L. Kesmodel
Department of Physics
Indiana University
Bloomington, Indiana 47403

Dr. K. C. Janda
California Institute of Technology
Division of Chemistry and Chemical Engineering
Pasadena, California 91125

Dr. E. A. Irene
Department of Chemistry
University of North Carolina
Chapel Hill, Northc Carolina 27514

Dr. Adam Heller
Bell Laboratories
Murray Hill, New Jersey 07974

Dr. Martin Fleischmann
Department of Chemistry
Southampton University
Southampton SO9 5NH
Hampshire, England

Dr. John W. Wilkins
Cornell University
Laboratory of Atomic and Solid State Physics
Ithaca, New York 14853

Dr. Richard Smardzewski
Code 6130
Naval Research Laboratory
Washington, D.C. 20375

Dr. H. Tachikawa
Chemistry Department
Jackson State University
Jackson, Mississippi 39217

ABSTRACTS DISTRIBUTION LIST, 056/625/629

Dr. R. G. Wallis
Department of Physics
University of California
Irvine, California 92664

Dr. D. Ramaker
Chemistry Department
George Washington University
Washington, D.C. 20052

Dr. J. C. Hemminger
Chemistry Department
University of California
Irvine, California 92717

Dr. T. F. George
Chemistry Department
University of Rochester
Rochester, New York 14627

Dr. G. Rubloff
IBM
Thomas J. Watson Research Center
P.O. Box 218
Yorktown Heights, New York 10598

Dr. Horia Metiu
Chemistry Department
University of California
Santa Barbara, California 93106

Captain Lee Myers
AFOSR/NC
Bollig AFB
Washington, D.C. 20332

Dr. J. T. Keiser
Department of Chemistry
University of Richmond
Richmond, Virginia 23173

Dr. Roald Hoffmann
Department of Chemistry
Cornell University
Ithaca, New York 14853

Dr. J. E. Jensen
Hughes Research Laboratory
3011 Malibu Canyon Road
Malibu, California 90265

Dr. J. H. Weaver
Department of Chemical Engineering
and Materials Science
University of Minnesota
Minneapolis, Minnesota 55455

Dr. R. W. Plummer
Department of Physics
University of Pennsylvania
Philadelphia, Pennsylvania 19104

Dr. E. Yeager
Department of Chemistry
Case Western Reserve University
Cleveland, Ohio 41106

Dr. N. Winograd
Department of Chemistry
Pennsylvania State University
University Park, Pennsylvania 16802

Dr. G. D. Stein
Mechanical Engineering Department
Northwestern University
Evanston, Illinois 60201

Dr. A. Steckl
Department of Electrical and
Systems Engineering
Rensselaer Polytechnic Institute
Troy, NewYork 12181

Dr. G. H. Morrison
Department of Chemistry
Cornell University
Ithaca, New York 14853

Dr. P. Hansma
Physics Department
University of California
Santa Barbara, California 93106

Dr. J. Baldeschwieler
California Institute of Technology
Division of Chemistry
Pasadena, California 91125

Dr. W. Goddard
California Institute of Technology
Division of Chemistry
Pasadena, California 91125

Dr. W. Knauer
Hughes Research Laboratory
3011 Malibu Canyon Road
Malibu, California 90265

Dr. C. B. Harris
Department of Chemistry
University of California
Berkeley, California 94720

DL/413/83/01
056/413-2

ABSTRACTS DISTRIBUTION LIST, 056/625/629

Dr. G. A. Somorjai
Department of Chemistry
University of California
Berkeley, California 94720

Dr. J. Murday
Naval Research Laboratory
Surface Chemistry Division (6170)
455 Overlook Avenue, S.W.
Washington, D.C. 20375

Dr. J. B. Hudson
Materials Division
Rensselaer Polytechnic Institute
Troy, New York 12181

Dr. Theodore E. Madey
Surface Chemistry Section
Department of Commerce
National Bureau of Standards
Washington, D.C. 20234

Dr. J. E. Demuth
IBM Corporation
Thomas J. Watson Research Center
P.O. Box 218
Yorktown Heights, New York 10598

Dr. M. G. Lagally
Department of Metallurgical
and Mining Engineering
University of Wisconsin
Madison, Wisconsin 53706

Dr. R. P. Van Duyne
Chemistry Department
Northwestern University
Evanston, Illinois 60637

Dr. J. M. White
Department of Chemistry
University of Texas
Austin, Texas 78712

Dr. D. E. Harrison
Department of Physics
Naval Postgraduate School
Monterey, California 93940

Dr. W. Kohn
Department of Physics
University of California, San Diego
La Jolla, California 92037

Dr. R. L. Park
Director, Center of Materials
Research
University of Maryland
College Park, Maryland 20742

Dr. W. T. Peria
Electrical Engineering Department
University of Minnesota
Minneapolis, Minnesota 55455

Dr. Keith H. Johnson
Department of Metallurgy and
Materials Science
Massachusetts Institute of Technology
Cambridge, Massachusetts 02139

Dr. S. Sibener
Department of Chemistry
James Franck Institute
5640 Ellis Avenue
Chicago, Illinois 60637

Dr. Arold Green
Quantum Surface Dynamics Branch
Code 3817
Naval Weapons Center
China Lake, California 93555

Dr. A. Wold
Department of Chemistry
Brown University
Providence, Rhode Island 02912

Dr. S. L. Bernasek
Department of Chemistry
Princeton University
Princeton, New Jersey 08544

Dr. P. Lund
Department of Chemistry
Howard University
Washington, D.C. 20059

END

FILMED

1-86

DTIC